ACS Photonics

pubs.acs.org/journal/apchd5

Article

Evidence for a Polariton-Mediated Biexciton Transition in Single-Walled Carbon Nanotubes

Jan M. Lüttgens, Zhuoran Kuang, Nicolas F. Zorn, Tiago Buckup,* and Jana Zaumseil*

Cite This: *ACS Photonics* 2022, 9, 1567−1576

Read Online

ACCESS | Metrics & More | Article Recommendations | Supporting Information

ABSTRACT: Strong coupling of excitonic resonances with a cavity gives rise to exciton−polaritons which possess a modified energy landscape compared to the uncoupled emitter. However, due to the femtosecond lifetime of the so-called bright polariton states and transient changes of the cavity reflectivity under excitation, it is challenging to directly measure the polariton excited state dynamics. Here, near-infrared pump−probe spectroscopy is used to investigate the ultrafast dynamics of exciton−polaritons based on strongly coupled (6,5) single-walled carbon nanotubes in metal-clad microcavities. We present a protocol for fitting the reflectivity-associated response of the cavity using genetic algorithm-assisted transfer-matrix simulations. With this approach, we are able to identify an absorptive exciton−polariton feature in the transient transmission data. This feature appears instantaneously under resonant excitation of the upper polariton but is delayed for off-resonant excitation. The observed transition energy and detuning dependence point toward a direct upper polariton-to-biexciton transition. Our results provide direct evidence for exciton−polariton intrinsic transitions beyond the bright polariton lifetime in strongly coupled microcavities.

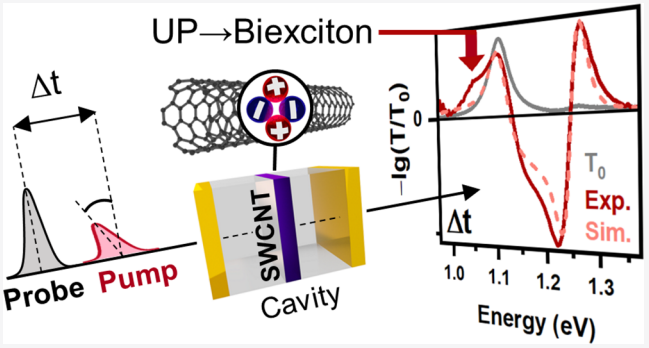

KEYWORDS: *microcavity, strong coupling, transient absorption, single-walled carbon nanotube, biexciton, transfer-matrix simulation*

Exciton−polaritons are hybrid light-matter quasiparticles that are formed when confined light interacts strongly with an excitonic resonance, e.g., in a metal-clad microcavity.[1,2] In this strong-coupling regime, mixed photon−exciton eigenstates arise that are called upper and lower polariton (UP and LP, respectively) with regard to the energy of the underlying excitonic transition. For molecular emitters, strong coupling offers new means to manipulate photophysical properties without chemical modification. Polariton states are readily tunable due to their photonic component and thus may provide alternative pathways for photoexcited processes, e.g., photocurrent generation[3−5] and spin conversion,[6−10] which has led to the efflorescence of the field of molecular polaritonics.[11] The delocalized photonic character of polaritons was also shown to improve energy transfer between spatially separated molecules[12,13] and long-range energy transport[14,15] in disordered molecular systems. To further improve and expand these applications of molecular polaritonics, it is essential to understand the fundamental properties of polaritonic states, especially their excited state dynamics.

The steady-state properties of strongly coupled macroscopic molecular systems are well-understood and can be modeled as coupled oscillators.[16] In such bulk systems, the Rabi splitting ($\hbar\Omega$) is a measure for the coupling strength, which scales with the square root of the number (N) of emitters (molecules) ($\hbar\Omega \propto \sqrt{N}$) in the cavity. One emitter state and the photon mode form the bright UP and LP modes, while $(N - 1)$ emitters form degenerate dark polariton states that are essentially molecular in nature.[17] The polariton steady state and the observable time-dependent fluorescence can be explained by the population of the bright polaritons from the so-called exciton reservoir by scattering[18] or nonadiabatic coupling (radiative pumping).[19−22] The exciton reservoir consists of dark polariton states and uncoupled molecular states.[23]

Despite these general insights, the specific conversion dynamics between exciton−polariton states (UP and LP) and molecular states have remained elusive.[24] This shortcoming is mainly due to a lack of suitable ultrafast spectroscopy methods. Especially in metal-clad microcavities, the intrinsic polariton lifetime, as derived from linewidth, ranges from a few to tens of femtoseconds.[25] This timescale is comparable to the shortest available laser pulses in the visible range and therefore not directly resolvable with conventional

Received: October 18, 2021
Published: May 4, 2022

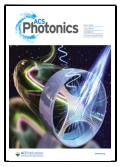

pump−probe measurements. Yet, the majority of the few studies on transient transmission and reflectivity of strongly coupled microcavities show that the overall response of the polariton modes is long-lived and emitter-like.[26−29] This effect can be attributed to the pump-induced bleach of the underlying emitter, which leads to a transient change of the emitter's complex refractive index and an associated transient transmission and reflectivity response that directly follows the emitter dynamics.[27,28] Depending on excitation conditions, thermal reflectivity of the metal mirrors[30] or transient changes of the cavity materials, such as the refractive index or layer thickness,[31] may further contribute to the cavity transient transmission and reflectivity response. Owing to these dominant, nonpolaritonic cavity transient effects, the evolution of the polariton population has not yet been extracted from pump−probe experiments with any certainty. Multiscale molecular dynamics simulations have shown that the short-lived bright polariton states may transfer population to the long-lived dark polariton states reversibly, thus elongating the bright polariton lifetime.[32] A two-dimensional Fourier transform spectroscopy study could confirm coherent energy exchange between UP, LP, and exciton reservoir during the first 100−150 fs after excitation.[24] However, for dynamics that take place after dephasing between photon and molecular components, no polariton intrinsic features, i.e., spectral signatures that are not merely the result of the transient change of the emitter's refractive index, have yet been observed.[26−29]

Here, we investigate the ultrafast dynamics of polariton states by fitting the emitter-bleach associated transient response of the system to identify absorptive features that are directly connected to the evolution of the polariton population. We study these effects for metal-clad microcavities with polymer-sorted (6,5) single-walled carbon nanotubes (SWCNTs). (6,5) SWCNTs are one-dimensional semiconductors with a band gap of about 1.27 eV, absorbing and emitting near-infrared light.[33] Purified semiconducting carbon nanotubes have emerged recently as an excellent material to create exciton−polaritons in planar microcavities[21,34−36] as well as in plasmonic lattices[37,38] due to their large oscillator strength, stable excitons with large binding energies, narrow absorption (E_{11}, E_{22}, etc.) and emission (only E_{11}) peaks with a small Stokes shift. Even ultrastrong coupling, electrical tuning and excitation of these SWCNT polaritons are easily achieved.[35,39,40]

Furthermore, SWCNTs exhibit intriguing photophysics and dynamics that have been studied in detail by transient absorption and other time-resolved spectroscopies.[41−44] The large Coulomb interactions in one-dimensional nanotubes and the reduced dielectric screening enable many-body bound states such as trions or biexcitons. Trions are charged excitons that occur in doped nanotubes[45−47] but can also be created optically at high excitation intensities.[48] For (6,5) SWCNTs, they show red-shifted (by 170−190 meV from E_{11}) absorption and emission. Biexcitons are bound states of two excitons and are often observed in zero-dimensional systems (e.g., quantum dots[49]) as well as nanotubes.[50,51] They are usually produced by the collision of two excitons but can also be created from an existing exciton population by absorption of additional photons. Hence, they are observable as an induced absorption feature in transient absorption measurements, which is red-shifted from the E_{11} exciton by about 130 meV for (6,5) SWNTs, as shown previously.[52,53]

By comparing the ultrafast transient transmission spectra of strongly coupled (6,5) SWCNTs in metal-clad cavities with genetic algorithm-assisted transfer-matrix simulations, we identify an exciton−polariton absorptive feature. Under resonant UP excitation, we observe this feature instantaneously at an energy matching a direct UP-to-biexciton transition. For nonresonant excitation, the proposed UP-to-biexciton transition is retained but occurs at later times. This indicates efficient population transfer between UP and dark polariton states for suitable detunings with strong overlap between UP and dark states.

RESULTS AND DISCUSSION

Cavity-Properties and Steady-State Data. Monochiral, polymer-sorted (6,5) SWCNTs were used as the active excitonic material in a metal-clad Fabry−Pérot cavity. These (6,5) nanotubes exhibit distinct absorption lines corresponding to the transitions to the excitonic states E_{11} (1.232 eV) and E_{22} (2.160 eV), with emission only from the E_{11} state (see reference film absorbance and emission in Figure S1). For the fabrication of the cavity (schematically shown in Figure 1a), a

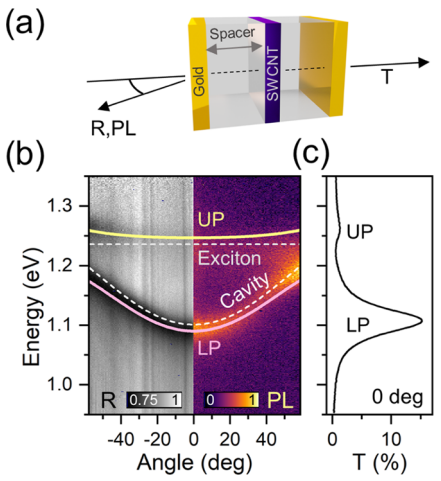

Figure 1. Strongly coupled (6,5) SWCNTs in a metal-clad microcavity. (a) Schematic of the sample structure and detection geometry. (b) Angle-resolved steady-state reflectivity (R) and photoluminescence (PL) of (6,5) SWCNTs in a planar cavity. The polariton modes (UP and LP) and cavity dispersion of a coupled oscillator fit to the reflectivity data are indicated as colored lines. (c) Steady-state transmission (T) of the same cavity at normal incidence.

dense and homogeneous (6,5) SWCNT film (thickness 30−40 nm) was spin-coated from a highly concentrated dispersion onto a gold-coated (30 nm) glass substrate with an aluminum oxide (AlO_x) spacer (120 nm, see Methods for details). After the formation of the nanotube layer, another AlO_x spacer (120 nm) and a top gold (30 nm) mirror were deposited. A (6,5) SWCNT reference film was deposited under the same conditions but without the mirrors and protected with 120 nm AlO_x for comparability. The cavity tuning was determined by the spacer layer thickness. By concentrating the nanotubes at the field maximum of the $\lambda/2$ cavity, the number of uncoupled emitters was reduced.

Figure 1b depicts the p-polarized angular dispersion of reflectivity (R) and photoluminescence (PL) for such a microcavity as recorded by Fourier imaging (see Methods for details). The reflectivity data exhibits a clear anti-crossing at

https://doi.org/10.1021/acsphotonics.1c01590
ACS Photonics 2022, 9, 1567−1576

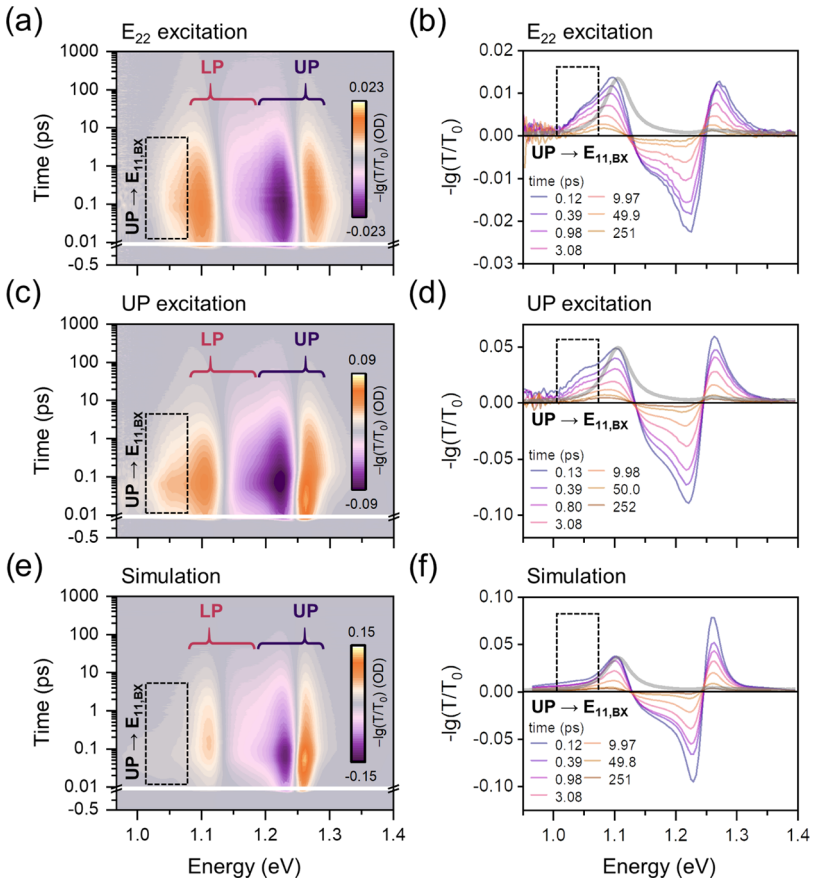

Figure 2. UP-to-biexciton ($E_{11,BX}$) transition as an intrinsic polariton ESA feature. (a, b) Transient transmission (TT) data of a strongly coupled SWCNT microcavity excited off-resonantly at the E_{22} exciton. (c, d) TT data of the same cavity resonantly excited at the UP mode. (e, f) Simulated TT data based on the transient absorption of a SWCNT reference film. The spectral regions of LP (red) and UP (dark purple) responses are indicated with the bracket tip pointing at the respective steady-state peak positions. The proposed UP-to-biexciton transition (UP → $E_{11,BX}$) is indicated by a dashed outline. The gray solid lines represent the steady-state transmissions of the cavities (b, d, f).

the coupled (6,5) SWCNT exciton (E_{11}, 1.232 eV), indicative of strong coupling. The UP and LP modes were fitted to the reflectivity data with the coupled oscillator model (see Methods for details), yielding a Rabi splitting of 80 meV. The quality factor estimated from the LP linewidth was $Q \approx 25$, corresponding to an ultrashort cavity lifetime of 15 fs. For the detuning chosen here (−140 meV), the UP strongly overlaps with the E_{11} absorption, leading to efficient coupling to the polariton dark states (DS),[32] whereas the LP mainly overlaps with the (6,5) SWCNT emission sidebands (Figure S1b). As a consequence, no emission is observed from the UP,[54] while the LP emits efficiently (see PL in Figure 1b) for energies with maximum overlap between LP and the (6,5) SWCNT photoluminescence tail and sidebands, as reported previously.[21] Note that the PL decay from the LP follows approximately the PL decay dynamics of (6,5) SWCNTs without a cavity (see Figure S2) because the LP fluorescence decay is limited by the slow population from the dark states that possess a similar lifetime as the weakly coupled SWCNT excitons.

Figure 1c shows the steady-state transmission (T) at normal incidence of the same cavity, given as a reference to identify the transient features of the UP and LP mode in the following. Note that the LP transmission peak (Figure 1c) appears broader than the LP in reflectivity due to the color scale in Figure 1b. A superposition of transmission and reflectivity data can be found in the Supporting Information (Figure S3).

Transient Transmission Data. The polariton dynamics were investigated by applying pump−probe spectroscopy in a transmission geometry. The transient absorption (TA) data of a (6,5) SWCNT film sandwiched between two aluminum oxide layers (Figure S4) serves as a reference for the emitter dynamics in the weak coupling regime. Cavity-embedded SWCNTs and reference SWCNTs were subjected to the same excitation power. For this, the reference was excited with lower pulse energies (2 nJ) and the cavity with higher pulse energies (30 nJ) to account for excitation losses (∼93%) at the top mirror of the cavity sample. Before analyzing the experimental transient transmission (TT) data, it is important to consider the variations in reflectivity during and after excitation, as the corresponding change in sample transmission is convoluted with the change in absorption.

The transient change in reflectivity of the reference sample is negligible, as the PFO-BPy matrix and AlO_x layers are transparent at the excitation wavelength (575 nm) and the excitation density (4 μJ cm^{-2}) is too low for nonlinear processes such as multi-photon absorption, which could affect the refractive index and, consequently, the reflectivity. For the strongly coupled cavity, the reflectivity contributions have to be separated from polariton excited state absorption (ESA). For metal-clad cavities, the dominant contribution is thermal excitation of the cavity mirrors,[30] especially the top mirror, which interacts with the unattenuated pump pulse. For the applied experimental parameters, this effect is small in our

https://doi.org/10.1021/acsphotonics.1c01590
ACS Photonics 2022, 9, 1567−1576

samples (<1 mOD, see Figure S5, together with a discussion of potential thermal expansion of the adjacent spacer layer). Furthermore, about 93% of the pump pulse is reflected at the top mirror, the pump fluence incident on the dielectric layers is again low (4−40 μJ cm^{-2}) and nonlinear effects can be disregarded. Note that under different excitation conditions, the dielectric layers might be affected by the excitation pulse.[31]

Based on the reasoning above, the change in reflectivity is dominated by the bleach of the SWCNTs, leading to an emitter-like component in the transient response of LP and UP. This emitter-like component of the corresponding cavity transient transmission was determined by transfer-matrix (TM) simulation. The transient change in the complex refractive index of the emitter layer was extracted from the transient absorption of the SWCNT reference using Kramers−Kronig relation[27] and employed to calculate the optical response of the strongly coupled sample for each pump−probe delay (for details, see Supporting Information, Figure S6). To account for small variations in the SWCNT film and in the cavity layers, a genetic algorithm was used to optimize the structural input parameters for the TM simulation (e.g., layer thicknesses and layer roughness) to fit the investigated area of the cavity sample (for details see Supporting Information, Figures S6 and S7 and Tables S1 and S2). By comparing the experimental and simulated TT data, we were able to identify intrinsic polariton features, as they are not contained in the TM simulation, which was purely based on the transient refractive index change of the weakly coupled emitter.

Figure 2a,b depicts the experimental TT data, given as $\Delta T = -\lg(T/T_0)$ of the strongly coupled cavity described above when excited off-resonantly at the SWCNT E_{22} exciton transition. The spectrum exhibits two positive and one negative components that decay at similar rates over a few hundred picoseconds. The region from 1.05 to 1.18 eV can be attributed to the LP ground-state response and the region from 1.18 to 1.3 eV to the UP ground-state response. These features can be interpreted as follows. The pump pulse promotes ground-state population to the E_{22} exciton manifold, and the resulting ground-state bleach reduces the absorption at the E_{11} transition, leading to a reduction in Rabi splitting, as shown in Figure S8. For the UP mode, this leads to an increase in transmission (purple) below 1.25 eV and a decrease in transmission (orange) above 1.25 eV as the UP mode is shifted toward lower energies. The same process occurs for the LP around 1.13 eV, with inverse signs. After the arrival of the pump pulse, the ground-state population recovers and the Rabi splitting increases again, which is monitored by the probe pulse. This process produces the characteristic derivative-like lineshape in the transient polariton response of the polariton ground state (compare Figure 2b,d,f with Figure S8), which is ubiquitous in strongly coupled Fabry−Pérot cavities.[27,28,55] Note that within the probed time window, the LP shifts exclusively to lower energies and the UP to higher energies, approaching their equilibrium positions observed in steady-state transmission. The TM simulation (see Figure 2e,f) captures this behavior quite accurately without invoking polariton excited state dynamics.

Further comparing the experimental data (Figure 2b) to the simulation (Figure 2f), we find slightly broader lineshapes for the former, mostly because in the simulation, the interface roughness was modeled by a global scalar scattering parameter and scattering within the layers was neglected. Despite the overall good agreement between the TM scheme and experiment at later times (>1 ps), larger discrepancies are found at early times (<1 ps, see Figure S9a,b). One cause for this mismatch may be the more prominent role of equilibration between UP, LP, and dark polariton states, which has been predicted to evolve over the first few hundred femtoseconds (100−200 fs) for direct excitation of the emitter in the case of small molecules.[32] Another cause for this mismatch is the omission of the coherent interaction between pump and probe pulse at early times (<100 fs). At later times, we expect the mismatches to arise from the intrinsic polariton dynamics not included in the simulation.

Importantly, there is an unexpected red-shifted shoulder of the LP response in the experimental data of the strongly coupled cavity, which is completely absent in the simulation (compare Figure 2a with Figures 2e and S9c,d). The origin of this shoulder cannot be explained by a transient change of transmission. First, the LP shifts exclusively to lower energies toward its equilibrium position. Hence, transitions lower in energy than the steady-state LP transition indicate ESA. Second, weakly coupled SWCNT-related ESA that may be observable through the red flank of the LP is accounted for by the simulated TT spectrum. This is shown in Figure S9c, where the experimental TT spectrum is superimposed onto the simulation and steady-state transmission. Hence, the observed shoulder must originate from polariton ESA.

The spectral position of the shoulder (1.05 eV) equals approximately the energy separation between the UP and the E_{11} biexciton (BX) of the (6,5) SWCNTs, which we estimated to be around 1.07 eV ($2E_{11}$(1.23 eV) − E_{UP}(1.26 eV) − E_{Bind}^{BX}(0.13 eV)) for this cavity sample. The biexciton binding energy (E_{Bind}^{BX}) was determined by Yuma et al. for surfactant-dispersed (6,5) SWCNTs in water.[53] Note that for PFO-BPy wrapped SWCNTs, the E_{11} energy is shifted to lower energies by 30 meV, as is the biexciton absorption (E_{11}(1.23 eV) − E_{Bind}^{BX}(0.13 eV) = 1.1 eV, see the region around 1.1 eV for the reference film, Figure S4). We can exclude a transition into the SWCNT trion because trions were only observed in the TA of chemically doped PFO-BPy-wrapped SWCNTs[47] and were also absent in the TA of the reference film. Consequently, the most dominant excited state transition in our system should be the E_{11} to biexciton transition and we therefore interpret the observed red-shifted shoulder in the cavity TT spectrum as a direct UP-to-biexciton transition.

To further test this assignment, the cavity sample was excited resonantly at the UP energy. Figure 2c,d depicts the corresponding TT data. Apart from the expected UP and LP ground-state features, the same red-shifted shoulder appears slightly more pronounced and at earlier times. In contrast to off-resonant excitation (Figure 2a,b), the UP is directly populated by the pump pulse, which is consistent with an immediate onset of the proposed biexciton absorption.

The absorptive feature is also observed for direct excitation of the LP and with a slight delay of 45 fs (see Figure S10a,b). To the best of our knowledge, population transfer from the LP to the UP has not been reported for pure LP excitation (note that the pump width at the LP energy is about 25 meV). Although phonon-assisted nonadiabatic transitions among polariton states have recently been reported,[56] the question of how the large energy gap of −140 meV between LP and DS could be surpassed remains elusive and will be the subject of future work.

As seen in Figure 2a,b, the red-shifted shoulder indicates that there is UP population even after 1 ps, far beyond the

https://doi.org/10.1021/acsphotonics.1c01590
ACS Photonics 2022, 9, 1567−1576

intrinsic UP lifetime (~15 fs). Hence, the UP population must be replenished from a long-lived state, which should be the exciton reservoir or dark states. The interpretation of the UP population being the rate-limiting step for the observed UP-to-biexciton transition is similar to the explanation for the experimentally observed long-lived LP photoluminescence decays.[19−21] We tested this hypothesis by measuring a cavity with a thicker oxide spacer, i.e., a larger detuning, and a cavity with a thinner oxide spacer, i.e., a smaller detuning. For the larger detuning (−184 meV), we could still observe a red-shifted shoulder for the UP excitation (see Figure S11a), as the overlap between UP and exciton reservoir was not changed significantly compared to the data shown in Figure 2. However, for a smaller detuning (−33 meV), i.e., reduced overlap between the UP and the exciton reservoir, the shoulder vanished (see Figure S11b).

Decay Associated Difference Spectra (DADS). The experimental and simulated pump−probe data shown in Figure 2 can be further analyzed by global analysis. Without assuming any detailed kinetic model, the data is fitted globally (i.e., all wavelengths are fitted simultaneously) with a sum of exponentials, where the amplitudes depend on the wavelength. The number of exponentials is usually equal to the number of spectrally different components, e.g., electronic states, molecules, *etc.* The amplitude of each exponential is called decay associated difference spectrum (DADS).[57] All three datasets in Figure 2 could be described using five decays (1−5) and an offset accounting for measurement noise.

Figure 3 shows the respective DADS with the corresponding time constants (k_1−k_5) being summarized in Table 1. The global analysis again reveals the UP-to-biexciton transition (UP → $E_{11,BX}$) peak at around 1.05 eV for excitation at E_{22} or UP. This is especially clear in the second decay component k_2. In the case of UP excitation, the first two decays are about twice as fast as for E_{22} excitation. We attribute the slower decays for E_{22} excitation to the delay caused by the required internal relaxation to the E_{11} state (~100 fs)[47] and subsequent population of the UP by the dark polariton states. This evolution of the proposed UP-to-biexciton transition approximately follows the evolution of the LP feature (at 1.1 eV in Figure 3a,b). As mentioned earlier, the LP feature is a direct consequence of the SWCNT ground-state bleach. Hence, the simultaneous spectral evolution of the UP and the LP feature indicates that the polariton-mediated biexciton transition follows the decay of the ground-state bleach. This is in agreement with previous experiments on weakly coupled (6,5) SWCNTs, in which the biexciton population followed the exciton population,[53] and further corroborates the biexciton character of the observed transition at 1.05 eV. Note that the k_2 and k_3 decay rates still contain the ground-state response. The UP-to-BX feature in the k_2 and k_3 spectra shows that for these time constants it is a contribution not that the UP-to-BX feature decays with precisely these rates.

The polariton intrinsic nature of the absorptive feature at 1.05 eV (Figure 2a−d) as an UP-to-biexciton transition is further corroborated by the global analysis of the simulated data (see Figure 3c). As described above, the simulated data does not contain any polariton intrinsic features and, therefore, the DADS shown in Figure 3c lack any feature at 1.05 eV. It is important to note that the TM simulation does not include any coherent interaction at early delay times between pump and probe (Δt < 0.5 ps), and the interpretation of the first component k_1 of the simulated data must be considered

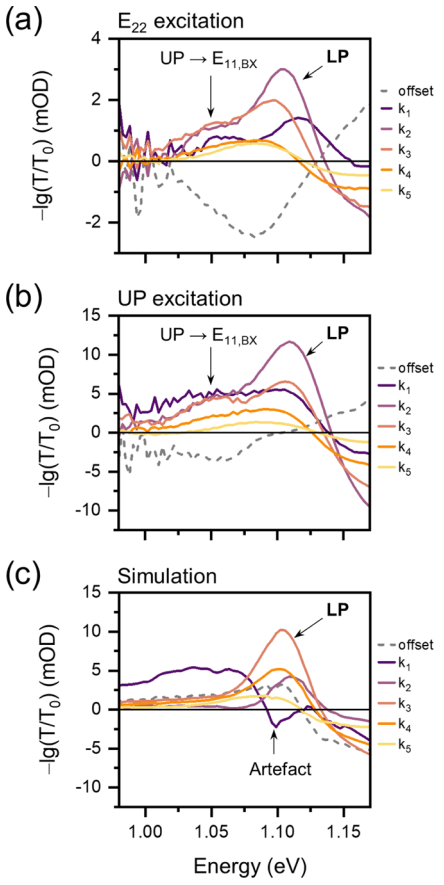

Figure 3. Biexciton absorption feature in decay associated difference spectra (DADS). (a) Strongly coupled (6,5) SWCNT microcavity excited off-resonantly at E_{22} (a), excited resonantly at the UP mode (b), and for a corresponding TM simulation (c). The extracted time constants (k_1−k_5) and lifetimes can be found in Table 1.

carefully. For example, the negative feature at the LP position (~1.1 eV, Figure 3c) is an obvious indication for the k_1 component to be unphysical. The slower components (k_2−k_5, Figure 3c), however, are not affected by artifacts and can be interpreted safely. Note that this only applies to the simulated data. The absence of the absorptive transition feature in these components of the simulated data corroborates that it is not caused by a change in transmission of the cavity stack and thus is indeed intrinsic to the polariton dynamics.

For the lifetimes calculated from the k_2 to k_5 components of the simulated data, we find similar values as for UP excitation (see Table 1). As the dynamics of the simulated data arise directly from the dynamics of the weakly coupled SWCNTs, the timescales covered by k_2 to k_5 are dominated by the emitter dynamics with regard to the polariton ground-state response (compare LP feature in Figure 3) in agreement with previous reports.[27,28] The consistently slower decays of k_3 to k_4 for E_{22} excitation are likely not polariton-related and an intrinsic feature of SWCNTs. For polymer-wrapped (6,5) SWCNTs in tetrahydrofuran, it was observed that the overall decay times were slightly elongated for excitation to higher excitonic levels such as the E_{22} or E_{33}.[47] The k_5 values should be essentially similar; however, the increased noise level at later times makes the fit less reliable, and the stated fit error likely underestimates the real uncertainty.

Kinetic Model and Implications for UP Population. We now assess the population of the UP state and the

https://doi.org/10.1021/acsphotonics.1c01590
ACS Photonics 2022, 9, 1567−1576

Table 1. Summary of Lifetimes $(1/k)$ Obtained by the Global Fit

lifetime component	$1/k_1$ (ps)	$1/k_2$ (ps)	$1/k_3$ (ps)	$1/k_4$ (ps)	$1/k_5$ (ps)
E_{22} excitation	0.53 ± 0.06	2.0 ± 0.2	10 ± 1	47 ± 6	380 ± 40
UP excitation	0.20 ± 0.02	1.15 ± 0.05	5.3 ± 0.2	38 ± 2	543 ± 40
simulation	0.127 ± 0.003	0.78 ± 0.03	4.06 ± 0.06	20.9 ± 0.2	328 ± 3

efficiency of the proposed polariton-mediated UP-to-biexciton transition. Figure 4a presents the kinetic model based on the previous discussion, including the ground state (GS), different excited (E_{11}, E_{22}, BX) and polaritonic (UP, LP, DS) states of strongly coupled (6,5) SWCNTs. Figure 4b shows the respective normalized time traces at the transition energy of the absorptive feature for resonant (at the UP) and off-resonant (at E_{22}) excitation, and the exciton-to-biexciton transition of the reference film. For resonant excitation at the UP, the maximum population is reached after around 60 fs within the experimental time-resolution (instrument response function ~90 fs). This indicates that the transition is connected to the UP population, of which a significant fraction should decay within the instrument response time. For off-resonant excitation at the E_{22} transition, the maximum population is reached after around 130 fs, indicating that the transition is delayed by internal relaxation and population of the DS and, subsequently, the UP. The fast decay of the biexciton population within the first 150 fs observed for UP excitation is absent for off-resonant E_{22} excitation. In the former scenario, the population is injected directly into the UP from which the product states (which we propose to be the biexciton) can be populated efficiently at early times. After 150 fs, a considerable UP population is lost due to relaxation into the dark states as inferred from PL measurements (see Figure 1b). From then on, the proposed UP-to-biexciton transition feature evolves similar to off-resonant E_{22} excitation. Thus, we assume that the UP-to-dark state relaxation must be dominant while the UP is constantly repopulated from the dark states at a slower rate. The resulting finite population can explain the slow decay of the UP-to-biexciton transition at rates similar to the biexciton feature in the reference film.

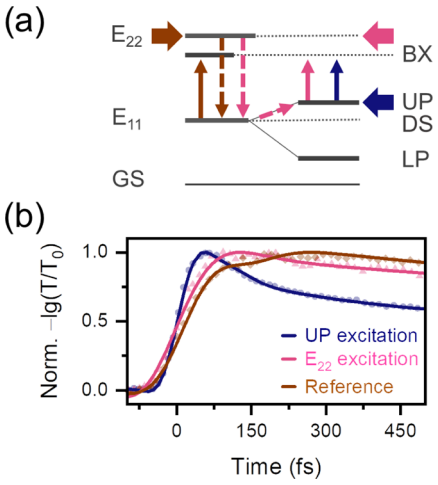

Figure 4. (a) Kinetic model for polariton-assisted biexciton transition by resonant (UP, blue) and off-resonant (E_{22}, pink) excitation in comparison to the SWCNT reference (brown). (b) Fitted time traces of the biexciton absorption in the reference film (extracted at exciton-to-biexciton energy) and strongly coupled cavity (extracted at the transition energy of the absorptive feature) with color-coding for the respective experimental conditions.

As mentioned earlier, the connection between UP and dark states can be tested by changing the overlap between the two states, i.e., the detuning of the cavity. For more negative detunings (still with similar overlap between UP and dark states), the UP-to-biexciton transition is still observed, whereas, for less negative detuning, the transition vanishes (Figure S11).

The latter also underlines that the DS-to-UP transition is entropically and enthalpically disfavored if the overlap between DS and UP is small and the energy barrier is high.[58] Yet, for a highly negative detuning, the DS-to-UP transition becomes competitive compared to the reverse process.

Due to the spectral overlap between UP-to-BX transition and LP ground-state response, the kinetics of the UP-to-BX cannot be extracted from the experimental cavity data of Figure 4. However, for a DS-to-UP rate of $(150\ \text{fs})^{-1}$ and a bright polariton decay rate of $(15\ \text{fs})^{-1}$, the kinetic model proposed above yields an evolution of the UP population that is similar to the experimental time traces of the UP-to-BX transition (see Figure S12). The kinetic model also shows that the UP population may have a lifetime in the picosecond range if efficient population exchange with the DS is possible.

The efficiency of the proposed UP-to-biexciton transition can be estimated by comparing the absolute signal intensities between cavity and reference sample at the respective biexciton features (see the Supporting Information, Figure S13). This comparison reveals that the UP-to-biexciton transition feature is 3 times more intense for the strongly coupled sample under E_{22} excitation than for the reference. For resonant excitation of the UP, the transition efficiency can be increased further up to 4-fold compared to off-resonant excitation, as the dark states are bypassed. Note that this is the case even though the E_{22} excitation should be 17% more efficient based on the calculated electromagnetic field intensity inside the cavity (see the Supporting Information, Figure S14).

CONCLUSIONS

By analyzing and comparing the transient transmission response of strongly coupled (6,5) SWCNTs in metal-clad microcavities with genetic algorithm-assisted transfer-matrix simulations, we were able to identify an intrinsic exciton−polariton absorptive feature. The transition energy and kinetics of this feature point toward a direct upper polariton-to-biexciton transition. This transition is 3 times more efficient than the biexciton transition in a weakly coupled reference. It is present for both resonant UP and nonresonant excitation at E_{22}, however, only for detunings at which the UP can efficiently exchange population with the dark states. The kinetics of the observed polariton-mediated absorptive feature imply that the UP can be repopulated by the dark states to a significant extent, thus increasing the UP population lifetime to the picosecond range despite the ultrashort intrinsic UP lifetime. These observations underline the need for tracing the polariton population in such systems directly. Transfer-matrix

https://doi.org/10.1021/acsphotonics.1c01590
ACS Photonics 2022, 9, 1567−1576

simulations assisted by global optimization methods, as shown here for a genetic algorithm, can be powerful tools to analyze the corresponding data with greater reliability and thus help to identify and investigate polariton-intrinsic transitions.

METHODS

Selective Dispersion of (6,5) SWCNTs and Film Preparation. As reported previously,[59] (6,5) SWCNTs were selectively extracted from CoMoCAT raw material (Chasm Advanced Materials, SG65i-L58, 0.38 g L^{-1}) by polymer wrapping with PFO-BPy (poly[(9,9-dioctylfluorenyl-2,7-diyl)-alt-(6,6′-(2,2′-bipyridine))], American Dye Source, M_w = 40 kg mol^{-1}, 0.5 g L^{-1}) in toluene using a shear force mixing process (Silverson L2/Air, 10 230 rpm, 72 h). The impurities were removed by centrifugation at 60,000g (Beckman Coulter Avanti J26XP centrifuge) for 2 × 45 min with intermediate supernatant extraction. The resulting dispersion was passed through a PTFE membrane filter (Merck Millipore, JVWP, 0.1 μm pore size) to collect the nanotubes and remove excess polymer. The filter cakes were peeled from the PTFE membrane and washed three times with toluene at 80 °C for 15 min before 0.8 mL of a 2 g L^{-1} PFO-BPy solution in toluene was added, and the mixture was sonicated for 1 h. Subsequently, 0.2 mL of toluene was added in 50-μL steps, each followed by 15 min sonication until a homogeneous liquid with a honey-like viscosity was obtained and used for film formation, resulting in about 1.1 wt % of (6,5) SWCNT in the film.

Microcavity Fabrication. The microcavity shown in Figure 1a was prepared on a clean glass substrate (Schott AF32eco, 300 μm) with a 2 nm chromium adhesion layer and a 30 nm thick thermally evaporated gold bottom mirror. A spacer layer of AlO_x (120 nm) was deposited by atomic layer deposition (Ultratech, Savannah S100, precursor trimethylaluminium, Strem Chemicals, Inc.) at 80 °C. The SWCNT layer (see above) was spin-coated at 800 rpm, followed by another AlO_x (120 nm) space layer and a 30 nm gold top mirror. The reference sample was prepared likewise but without gold mirrors.

Steady-State Measurements. Transmission spectra were recorded with a V-770 (JASCO) spectrophotometer. For angle-resolved reflectivity measurements, a white light source (Ocean Optics, HL-2000-FHSA) was focused onto the sample by an infinity corrected ×100 nIR objective with 0.85 NA (Olympus, LCPLN100XIR). The resulting spot diameter of ∼2 μm defined the investigated area on the sample. For angle-resolved PL, the white light source was replaced with a 640 nm laser diode (Coherent OBIS, 5 mW, continuous wave) and the reflected laser light was blocked by an 850 nm cutoff long-pass filter. The reflected/emitted light from the sample was imaged onto the entrance slit of an imaging spectrometer (Princeton Instruments IsoPlane SCT 320) using a 4f Fourier imaging system (f_1 = 200 mm and f_2 = 300 mm). The resulting angle-resolved spectra were recorded with a 640 × 512 InGaAs array (Princeton Instruments, NIRvana:640ST). A linear polarizer was placed in front of the spectrometer to select between s and p polarization.

Time-Dependent PL Measurements. The spectrally filtered output of a picosecond-pulsed supercontinuum laser source (Fianium WhiteLase SC400) was focused onto the sample by an objective (Olympus, LCPLN100XIR) and imaged confocally onto an Acton SpectraPro SP2358 spectrograph (grating 150 lines mm^{-1}). A dichroic long-pass filter (830 nm cutoff) was used to block scattered laser light. A liquid nitrogen-cooled InGaAs line camera (Princeton Instruments OMA-V) was used for spectral acquisitions required to find the desired cavity emission spectrum. The spectrally filtered PL emission was then imaged onto a gated InGaAs/InP avalanche photodiode (Micro Photon Devices) via a ×20 nIR optimized objective (Mitutoyo). Photon arrival time statistics were acquired by a time-correlated single-photon counting module (PicoHarp 300, Picoquant GmbH). The instrument response function (IRF) was estimated by the detector-limited PL decay of a (6,5) SWCNT reference at the E_{11} transition.

Pump−Probe Measurements and Global Analysis. Femtosecond transient transmission (TT) and absorption (TA) measurements were performed with a commercial TA spectrograph (HELIOS Fire, Ultrafast Systems). The pump pulses were spectrally centered at 1000 and 576 nm and generated with a commercial optical parametric amplifier (TOPAS-PRIME, Light Conversion) that was pumped by a regeneratively amplified femtosecond Ti:Sapphire laser (Astrella, Coherent) centered at 800 nm, with a 4 kHz repetition rate, 78 fs pulse durations, and 1.6 mJ pulse energy. The spot size of the focused pump beam was about 250 μm at the sample position. Typically, pump fluences were 200 μJ cm^{-2} for pulse energies of 100 nJ. The supercontinuum probe beam was linearly polarized at the magic angle (54.7°) relative to the pump polarization. Experimental spectra were corrected for the group velocity dispersion of the broadband probe beam before analysis. All measurements were performed under ambient conditions. Time-resolved datasets were analyzed by standard global analysis, as described previously.[60] The number of exponentials was chosen to minimize fitting error and residual structure.

Data Analysis and Simulation. The angle-resolved reflectivity data was analyzed by a coupled oscillator model, as described previously.[21] In short, the UP and LP dispersions were fitted by the analytical expression for their energy eigenvalues

$$E_{UP/LP} = \frac{1}{2}(E_X - i\hbar\Gamma_X + E_C - i\hbar\Gamma_C) \pm \frac{1}{2}\sqrt{V_A{}^2 + 0.25(E_X - i\hbar\Gamma_X - E_C + i\hbar\Gamma_C)^2} \quad (1)$$

where E_X is the SWCNT E_{11} exciton energy and E_C is the cavity energy dispersion, which depends on the effective refractive index n_{eff} between the mirrors and the angle θ by $E_C(\theta) = E_0(1 - (\sin(\theta)/n_{eff})^2)^{-1/2}$. Γ_C and Γ_X are the half width at half maximum of the cavity and exciton resonance, respectively, and V_A is the coupling potential, which depends on the Rabi splitting $\hbar\Omega$ with $V_A = \sqrt{\hbar\Omega^2 + (i\hbar\Gamma_C - i\hbar\Gamma_X)^2}$.

Transfer-matrix simulations of the cavity transient transmission were performed based on complex refractive index data calculated from the TA data recorded for the SWCNT reference sample using Kramers−Kronig relations (Figure S6). The input parameters, i.e., the layer thicknesses of the microcavity, the average interface roughness between layers, the fraction of ground-state bleach and a scaling parameter, were extracted by fitting the experimental differential transmission spectrum at a pump−probe delay of 10 ps for a microcavity excited at the same pump wavelength as the reference using a genetic algorithm (Figure S7 and Tables S1

https://doi.org/10.1021/acsphotonics.1c01590
ACS Photonics 2022, 9, 1567−1576

and S2). The quality of the fit was assessed by comparing the fitted layer thicknesses and interface roughness with experimental values obtained from atomic force micrographs (Bruker Dimension Icon, tapping mode) of reference layers fabricated under the same conditions as the cavity layers (see Table S2).

■ ASSOCIATED CONTENT

Supporting Information

The Supporting Information is available free of charge at https://pubs.acs.org/doi/10.1021/acsphotonics.1c01590.

Absorption and emission spectra of (6,5) SWCNT films, transient complex refractive index of metal mirrors, extraction of transient complex refractive index of the emitter layer, genetic algorithm-assisted transfer-matrix simulation of transient transmission data, additional transient transmission data, kinetic model, and biexciton transition efficiency data (PDF)

■ AUTHOR INFORMATION

Corresponding Authors

Tiago Buckup − *Institute for Physical Chemistry, Universität Heidelberg, D-69120 Heidelberg, Germany; Centre for Advanced Materials, Universität Heidelberg, D-69120 Heidelberg, Germany;* orcid.org/0000-0002-1194-0837; Email: tiago.buckup@pci.uni-heidelberg.de

Jana Zaumseil − *Institute for Physical Chemistry, Universität Heidelberg, D-69120 Heidelberg, Germany;* orcid.org/0000-0002-2048-217X; Email: zaumseil@uni-heidelberg.de

Authors

Jan M. Lüttgens − *Institute for Physical Chemistry, Universität Heidelberg, D-69120 Heidelberg, Germany*

Zhuoran Kuang − *Institute for Physical Chemistry, Universität Heidelberg, D-69120 Heidelberg, Germany; Centre for Advanced Materials, Universität Heidelberg, D-69120 Heidelberg, Germany;* orcid.org/0000-0002-1594-8107

Nicolas F. Zorn − *Institute for Physical Chemistry, Universität Heidelberg, D-69120 Heidelberg, Germany;* orcid.org/0000-0001-9651-5612

Complete contact information is available at: https://pubs.acs.org/10.1021/acsphotonics.1c01590

Notes

The authors declare no competing financial interest.

■ ACKNOWLEDGMENTS

This research was funded by the VolkswagenStiftung (Grant No. 93404). N.F.Z. and J.Z. also acknowledge funding from the European Research Council (ERC) under the European Union's Horizon 2020 research and innovation programme (Grant Agreement No. 817494, "TRIFECTs").

■ REFERENCES

(1) Weisbuch, C.; Nishioka, M.; Ishikawa, A.; Arakawa, Y. Observation of the Coupled Exciton-Photon Mode Splitting in a Semiconductor Quantum Microcavity. *Phys. Rev. Lett.* **1992**, *69*, 3314−3317.

(2) Lidzey, D. G.; Bradley, D. D. C.; Skolnick, M. S.; Virgili, T.; Walker, S.; Whittaker, D. M. Strong Exciton−Photon Coupling in an Organic Semiconductor Microcavity. *Nature* **1998**, *395*, 53−55.

(3) Eizner, E.; Brodeur, J.; Barachati, F.; Sridharan, A.; Kéna-Cohen, S. Organic Photodiodes with an Extended Responsivity Using Ultrastrong Light−Matter Coupling. *ACS Photonics* **2018**, *5*, 2921−2927.

(4) Nikolis, V. C.; Mischok, A.; Siegmund, B.; Kublitski, J.; Jia, X.; Benduhn, J.; Hörmann, U.; Neher, D.; Gather, M. C.; Spoltore, D.; Vandewal, K. Strong Light-Matter Coupling for Reduced Photon Energy Losses in Organic Photovoltaics. *Nat. Commun.* **2019**, *10*, No. 3706.

(5) Mischok, A.; Lüttgens, J.; Berger, F.; Hillebrandt, S.; Tenopala-Carmona, F.; Kwon, S.; Murawski, C.; Siegmund, B.; Zaumseil, J.; Gather, M. C. Spectroscopic near-Infrared Photodetectors Enabled by Strong Light−Matter Coupling in (6,5) Single-Walled Carbon Nanotubes. *J. Chem. Phys.* **2020**, *153*, No. 201104.

(6) Stranius, K.; Hertzog, M.; Börjesson, K. Selective Manipulation of Electronically Excited States through Strong Light−Matter Interactions. *Nat. Commun.* **2018**, *9*, No. 2273.

(7) Eizner, E.; Martínez-Martínez, L. A.; Yuen-Zhou, J.; Kéna-Cohen, S. Inverting Singlet and Triplet Excited States Using Strong Light-Matter Coupling. *Sci. Adv.* **2019**, *5*, No. eaax4482.

(8) Berghuis, A. M.; Halpin, A.; Le-Van, Q.; Ramezani, M.; Wang, S.; Murai, S.; Gómez Rivas, J. Strong Light-Matter Coupling: Enhanced Delayed Fluorescence in Tetracene Crystals by Strong Light-Matter Coupling. *Adv. Funct. Mater.* **2019**, *29*, No. 1901317.

(9) Polak, D.; Jayaprakash, R.; Lyons, T. P.; Martínez-Martínez, L. Á.; Leventis, A.; Fallon, K. J.; Coulthard, H.; Bossanyi, D. G.; Georgiou, K.; Petty, I. I. A. J.; Anthony, J.; Bronstein, H.; Yuen-Zhou, J.; Tartakovskii, A. I.; Clark, J.; Musser, A. J. Manipulating Molecules with Strong Coupling: Harvesting Triplet Excitons in Organic Exciton Microcavities. *Chem. Sci.* **2020**, *11*, 343−354.

(10) Yu, Y.; Mallick, S.; Wang, M.; Börjesson, K. Barrier-Free Reverse-Intersystem Crossing in Organic Molecules by Strong Light-Matter Coupling. *Nat. Commun.* **2021**, *12*, No. 3255.

(11) Feist, J.; Galego, J.; Garcia-Vidal, F. J. Polaritonic Chemistry with Organic Molecules. *ACS Photonics* **2018**, *5*, 205−216.

(12) Georgiou, K.; Michetti, P.; Gai, L.; Cavazzini, M.; Shen, Z.; Lidzey, D. G. Control over Energy Transfer between Fluorescent Bodipy Dyes in a Strongly Coupled Microcavity. *ACS Photonics* **2018**, *5*, 258−266.

(13) Zhong, X.; Chervy, T.; Zhang, L.; Thomas, A.; George, J.; Genet, C.; Hutchison, J. A.; Ebbesen, T. W. Energy Transfer between Spatially Separated Entangled Molecules. *Angew. Chem., Int. Ed.* **2017**, *56*, 9034−9038.

(14) Rozenman, G. G.; Akulov, K.; Golombek, A.; Schwartz, T. Long-Range Transport of Organic Exciton-Polaritons Revealed by Ultrafast Microscopy. *ACS Photonics* **2018**, *5*, 105−110.

(15) Hou, S.; Khatoniar, M.; Ding, K.; Qu, Y.; Napolov, A.; Menon, V. M.; Forrest, S. R. Ultralong-Range Energy Transport in a Disordered Organic Semiconductor at Room Temperature *via* Coherent Exciton-Polariton Propagation. *Adv. Mater.* **2020**, *32*, No. 2002127.

(16) Kavokin, A.; Baumberg, J. J.; Malpuech, G.; Laussy, F. P. *Microcavities*, 2nd ed.; Oxford University Press: Oxford, 2017.

(17) Keeling, J.; Kéna-Cohen, S. Bose−Einstein Condensation of Exciton-Polaritons in Organic Microcavities. *Annu. Rev. Phys. Chem.* **2020**, *71*, 435−459.

(18) Coles, D. M.; Michetti, P.; Clark, C.; Tsoi, W. C.; Adawi, A. M.; Kim, J.-S.; Lidzey, D. G. Vibrationally Assisted Polariton-Relaxation Processes in Strongly Coupled Organic-Semiconductor Microcavities. *Adv. Funct. Mater.* **2011**, *21*, 3691−3696.

(19) Lidzey, D. G.; Fox, A. M.; Rahn, M. D.; Skolnick, M. S.; Agranovich, V. M.; Walker, S. Experimental Study of Light Emission from Strongly Coupled Organic Semiconductor Microcavities Following Nonresonant Laser Excitation. *Phys. Rev. B* **2002**, *65*, No. 195312.

(20) Grant, R. T.; Michetti, P.; Musser, A. J.; Gregoire, P.; Virgili, T.; Vella, E.; Cavazzini, M.; Georgiou, K.; Galeotti, F.; Clark, C.; Clark, J.; Silva, C.; Lidzey, D. G. Efficient Radiative Pumping of Polaritons in a

Strongly Coupled Microcavity by a Fluorescent Molecular Dye. *Adv. Opt. Mater.* **2016**, *4*, 1615−1623.
(21) Lüttgens, J. M.; Berger, F. J.; Zaumseil, J. Population of Exciton−Polaritons *via* Luminescent sp^3 Defects in Single-Walled Carbon Nanotubes. *ACS Photonics* **2020**, *8*, 182−193.
(22) Hulkko, E.; Pikker, S.; Tiainen, V.; Tichauer, R. H.; Groenhof, G.; Toppari, J. J. Effect of Molecular Stokes Shift on Polariton Dynamics. *J. Chem. Phys.* **2021**, *154*, No. 154303.
(23) Litinskaya, M.; Reineker, P.; Agranovich, V. M. Fast Polariton Relaxation in Strongly Coupled Organic Microcavities. *J. Lumin.* **2004**, *110*, 364−372.
(24) Mewes, L.; Wang, M.; Ingle, R. A.; Börjesson, K.; Chergui, M. Energy Relaxation Pathways between Light-Matter States Revealed by Coherent Two-Dimensional Spectroscopy. *Commun. Phys.* **2020**, *3*, No. 157.
(25) Ebbesen, T. W. Hybrid Light−Matter States in a Molecular and Material Science Perspective. *Acc. Chem. Res.* **2016**, *49*, 2403−2412.
(26) Virgili, T.; Coles, D.; Adawi, A. M.; Clark, C.; Michetti, P.; Rajendran, S. K.; Brida, D.; Polli, D.; Cerullo, G.; Lidzey, D. G. Ultrafast Polariton Relaxation Dynamics in an Organic Semiconductor Microcavity. *Phys. Rev. B* **2011**, *83*, No. 245309.
(27) Schwartz, T.; Hutchison, J. A.; Léonard, J.; Genet, C.; Haacke, S.; Ebbesen, T. W. Polariton Dynamics under Strong Light-Molecule Coupling. *ChemPhysChem* **2013**, *14*, 125−131.
(28) Liu, B.; Menon, V. M.; Sfeir, M. Y. The Role of Long-Lived Excitons in the Dynamics of Strongly Coupled Molecular Polaritons. *ACS Photonics* **2020**, *7*, 2292−2301.
(29) Wang, S.; Chervy, T.; George, J.; Hutchison, J. A.; Genet, C.; Ebbesen, T. W. Quantum Yield of Polariton Emission from Hybrid Light-Matter States. *J. Phys. Chem. Lett.* **2014**, *5*, 1433−1439.
(30) Liu, B.; Menon, V. M.; Sfeir, M. Y. Ultrafast Thermal Modification of Strong Coupling in an Organic Microcavity. *APL Photonics* **2021**, *6*, No. 016103.
(31) Renken, S.; Pandya, R.; Georgiou, K.; Jayaprakash, R.; Gai, L.; Shen, Z.; Lidzey, D. G.; Rao, A.; Musser, A. J. Untargeted Effects in Organic Exciton−Polariton Transient Spectroscopy: A Cautionary Tale. *J. Chem. Phys.* **2021**, *155*, No. 154701.
(32) Groenhof, G.; Climent, C.; Feist, J.; Morozov, D.; Toppari, J. J. Tracking Polariton Relaxation with Multiscale Molecular Dynamics Simulations. *J. Phys. Chem. Lett.* **2019**, *10*, 5476−5483.
(33) Weisman, R. B.; Bachilo, S. M. Dependence of Optical Transition Energies on Structure for Single-Walled Carbon Nanotubes in Aqueous Suspension: An Empirical Kataura Plot. *Nano Lett.* **2003**, *3*, 1235−1238.
(34) Graf, A.; Tropf, L.; Zakharko, Y.; Zaumseil, J.; Gather, M. C. Near-Infrared Exciton-Polaritons in Strongly Coupled Single-Walled Carbon Nanotube Microcavities. *Nat. Commun.* **2016**, *7*, No. 13078.
(35) Gao, W.; Li, X.; Bamba, M.; Kono, J. Continuous Transition between Weak and Ultrastrong Coupling through Exceptional Points in Carbon Nanotube Microcavity Exciton−Polaritons. *Nat. Photonics* **2018**, *12*, 362−367.
(36) Dhavamani, A.; Haeberlé, L.; Wang, J.; Kéna-Cohen, S.; Arnold, M. S. Cavity-Mediated Hybridization of Bright and Dark Excitons in an Ultrastrongly Coupled Carbon Nanotube Microcavity. *ACS Photonics* **2021**, *8*, 2375−2383.
(37) Zakharko, Y.; Graf, A.; Zaumseil, J. Plasmonic Crystals for Strong Light−Matter Coupling in Carbon Nanotubes. *Nano Lett.* **2016**, *16*, 6504−6510.
(38) Zakharko, Y.; Rother, M.; Graf, A.; Hähnlein, B.; Brohmann, M.; Pezoldt, J.; Zaumseil, J. Radiative Pumping and Propagation of Plexcitons in Diffractive Plasmonic Crystals. *Nano Lett.* **2018**, *18*, 4927−4933.
(39) Möhl, C.; Graf, A.; Berger, F. J.; Lüttgens, J.; Zakharko, Y.; Lumsargis, V.; Gather, M. C.; Zaumseil, J. Trion-Polariton Formation in Single-Walled Carbon Nanotube Microcavities. *ACS Photonics* **2018**, *5*, 2074−2080.
(40) Graf, A.; Held, M.; Zakharko, Y.; Tropf, L.; Gather, M. C.; Zaumseil, J. Electrical Pumping and Tuning of Exciton-Polaritons in Carbon Nanotube Microcavities. *Nat. Mater.* **2017**, *16*, 911−917.
(41) Zhu, Z. P.; Crochet, J.; Arnold, M. S.; Hersam, M. C.; Ulbricht, H.; Resasco, D.; Hertel, T. Pump-Probe Spectroscopy of Exciton Dynamics in (6,5) Carbon Nanotubes. *J. Phys. Chem. C* **2007**, *111*, 3831−3835.
(42) Park, J.; Deria, P.; Therien, M. J. Dynamics and Transient Absorption Spectral Signatures of the Single-Wall Carbon Nanotube Electronically Excited Triplet State. *J. Am. Chem. Soc.* **2011**, *133*, 17156−17159.
(43) Amori, A. R.; Hou, Z.; Krauss, T. D. Excitons in Single-Walled Carbon Nanotubes and Their Dynamics. *Annu. Rev. Phys. Chem.* **2018**, *69*, 81−99.
(44) Miyauchi, Y. Photoluminescence Studies on Exciton Photophysics in Carbon Nanotubes. *J. Mater. Chem. C* **2013**, *1*, 6499−6521.
(45) Matsunaga, R.; Matsuda, K.; Kanemitsu, Y. Observation of Charged Excitons in Hole-Doped Carbon Nanotubes Using Photoluminescence and Absorption Spectroscopy. *Phys. Rev. Lett.* **2011**, *106*, No. 037404.
(46) Jakubka, F.; Grimm, S. B.; Zakharko, Y.; Gannott, F.; Zaumseil, J. Trion Electroluminescence from Semiconducting Carbon Nanotubes. *ACS Nano* **2014**, *8*, 8477−8486.
(47) Kuang, Z.; Berger, F. J.; Lustres, J. L. P.; Wollscheid, N.; Li, H.; Lüttgens, J.; Balcı Leinen, M.; Flavel, B. S.; Zaumseil, J.; Buckup, T. Charge Transfer from Photoexcited Semiconducting Single-Walled Carbon Nanotubes to Wide-Bandgap Wrapping Polymer. *J. Phys. Chem. C* **2021**, *125*, 8125−8136.
(48) Santos, S. M.; Yuma, B.; Berciaud, S.; Shaver, J.; Gallart, M.; Gilliot, P.; Cognet, L.; Lounis, B. All-Optical Trion Generation in Single-Walled Carbon Nanotubes. *Phys. Rev. Lett.* **2011**, *107*, No. 187401.
(49) Hu, Y. Z.; Koch, S. W.; Lindberg, M.; Peyghambarian, N.; Pollock, E. L.; Abraham, F. F. Biexcitons in Semiconductor Quantum Dots. *Phys. Rev. Lett.* **1990**, *64*, 1805−1807.
(50) Kammerlander, D.; Prezzi, D.; Goldoni, G.; Molinari, E.; Hohenester, U. Biexciton Stability in Carbon Nanotubes. *Phys. Rev. Lett.* **2007**, *99*, No. 126806.
(51) Colombier, L.; Selles, J.; Rousseau, E.; Lauret, J. S.; Vialla, F.; Voisin, C.; Cassabois, G. Detection of a Biexciton in Semiconducting Carbon Nanotubes Using Nonlinear Optical Spectroscopy. *Phys. Rev. Lett.* **2012**, *109*, No. 197402.
(52) Styers-Barnett, D. J.; Ellison, S. P.; Mehl, B. P.; Westlake, B. C.; House, R. L.; Park, C.; Wise, K. E.; Papanikolas, J. M. Exciton Dynamics and Biexciton Formation in Single-Walled Carbon Nanotubes Studied with Femtosecond Transient Absorption Spectroscopy. *J. Phys. Chem. C* **2008**, *112*, 4507−4516.
(53) Yuma, B.; Berciaud, S.; Besbas, J.; Shaver, J.; Santos, S.; Ghosh, S.; Weisman, R. B.; Cognet, L.; Gallart, M.; Ziegler, M.; Hönerlage, B.; Lounis, B.; Gilliot, P. Biexciton, Single Carrier, and Trion Generation Dynamics in Single-Walled Carbon Nanotubes. *Phys. Rev. B* **2013**, *87*, No. 205412.
(54) Neuman, T.; Aizpurua, J. Origin of the Asymmetric Light Emission from Molecular Exciton−Polaritons. *Optica* **2018**, *5*, No. 1247.
(55) Virgili, T.; Coles, D.; Adawi, A. M.; Clark, C.; Michetti, P.; Rajendran, S. K.; Brida, D.; Polli, D.; Cerullo, G.; Lidzey, D. G. Ultrafast Polariton Relaxation Dynamics in an Organic Semiconductor Microcavity. *Phys. Rev. B* **2011**, *83*, No. 245309.
(56) Qiu, L.; Mandal, A.; Morshed, O.; Meidenbauer, M. T.; Girten, W.; Huo, P.; Vamivakas, A. N.; Krauss, T. D. Molecular Polaritons Generated from Strong Coupling between Cdse Nanoplatelets and a Dielectric Optical Cavity. *J. Phys. Chem. Lett.* **2021**, *12*, 5030−5038.
(57) van Stokkum, I. H. M.; Larsen, D. S.; van Grondelle, R. Global and Target Analysis of Time-Resolved Spectra. *Biochim. Biophys. Acta* **2004**, *1657*, 82−104.
(58) Fassioli, F.; Park, K. H.; Bard, S. E.; Scholes, G. D. Femtosecond Photophysics of Molecular Polaritons. *J. Phys. Chem. Lett.* **2021**, *12*, 11444−11459.
(59) Graf, A.; Zakharko, Y.; Schießl, S. P.; Backes, C.; Pfohl, M.; Flavel, B. S.; Zaumseil, J. Large Scale, Selective Dispersion of Long

https://doi.org/10.1021/acsphotonics.1c01590
ACS Photonics 2022, 9, 1567−1576

Single-Walled Carbon Nanotubes with High Photoluminescence Quantum Yield by Shear Force Mixing. *Carbon* **2016**, *105*, 593−599.
(60) Alagna, N.; Lustres, J. L. P.; Roozbeh, A.; Han, J.; Hahn, S.; Berger, F. J.; Zaumseil, J.; Dreuw, A.; Bunz, U. H. F.; Buckup, T. Ultrafast Singlet Fission in Rigid Azaarene Dimers with Negligible Orbital Overlap. *J. Phys. Chem. B* **2020**, *124*, 9163−9174.

https://doi.org/10.1021/acsphotonics.1c01590
ACS Photonics 2022, 9, 1567−1576